Classical-to-quantum transition in multimode nonlinear systems with strong photon-photon coupling

Yue-Xun Huang,[1,2] Ming Li,[1,2,*] Ke Lin,[3] Yan-Lei Zhang,[1,2] Guang-Can Guo,[1,2] and Chang-Ling Zou[1,2,†]

[1]*CAS Key Laboratory of Quantum Information, University of Science and Technology of China, Hefei 230026, People's Republic of China*

[2]*CAS Center For Excellence in Quantum Information and Quantum Physics, University of Science and Technology of China, Hefei, Anhui 230026, People's Republic of China*

[3]*School of Software, Tsinghua University, Beijing 100084, China*

(Received 16 December 2021; revised 11 March 2022; accepted 25 March 2022; published 7 April 2022)

With advanced micro- and nanophotonic structures, the vacuum photon-photon coupling rate is anticipated to approach the intrinsic loss rate and lead to unconventional quantum effects. Here, we investigate the classical-to-quantum transition of such photonic nonlinear systems using the quantum cluster-expansion method, which addresses the computational challenge in tracking large photon number states of the fundamental and harmonic optical fields involved in the second-harmonic generation process. Compared to the mean-field approximation used in the weak-coupling limit, the quantum cluster-expansion method solves multimode dynamics efficiently and reveals the quantum behaviors of optical parametric oscillations around the threshold. This paper presents a universal tool to study quantum dynamics of multimode systems and explore the nonlinear photonic devices for continuous-variable quantum information processing.

DOI: 10.1103/PhysRevA.105.043707

I. INTRODUCTION

Nonlinear optics has been exploited in abundant classical and quantum optics applications since the advent of lasers [1,2]. Under the current theoretical framework, the simplest approach to describe a coherent optical field is by characterizing it with only one parameter, i.e., the field amplitude, with the system dynamics governed by a set of nonlinearly coupled equations among modes of different amplitudes. This treatment, known as the mean-field approximation (MFA) [3], however, neglects the influence of quantum fluctuations. In a more rigorous framework, the optical fields are treated as Gaussian states for which the mean-field amplitude and second-order correlations are assumed to be complete to describe the system [4,5]. Then, the quantum fluctuations and correlations of optical fields can be derived by calculating the covariance matrix. In the past decades, the MFA and Gaussian-state approximation have been widely applied in quantum optics and successfully predict a variant of phenomena, including squeezing [6], continuous-variable entanglement [7], and the thermal dynamics of mechanical resonators [8,9].

In conventional nonlinear optics systems, the nonlinear coupling strengths between optical modes are much weaker than the dissipation rates, therefore the higher-order correlations between modes are negligible due to the strong decoherence, and the Gaussian state approximation is accurate. As the fabrication technique and material improve, the photon-photon coupling in the nonlinear system can be greatly enhanced, to the point that the single-photon nonlinearity becomes appreciable in photonic integrated circuits. The coupling strength to dissipation rate ratio g/κ has been greatly boosted during the last decades [10], using a microresonator made by gallium arsenide [11], aluminum nitride [12], indium gallium phosphide [13], lithium niobate [14–16], etc. For example, Lu *et al.* demonstrated a g/κ ratio over 1% in a periodically poled lithium niobate microring resonator [17], suggesting significant nonlinear effects at the level of tens of photons. At this high nonlinearity limit, the Gaussian state approximation no longer holds. With even larger g/κ, the nonlinear system is predicted to exhibit atomlike features [18,19], thus significant quantum effects arise under excitation at the single-photon level [20,21]. It is intriguing to explore the classical-to-quantum transition in this new regime where g/κ approaches unity and the conventional treatment of high amplitude bosonic modes under MFA is no longer valid, and the quantum master equation with truncated Fock-state dimension becomes inefficient. It has been demonstrated that a quantum state can be also represented by the correlation of operators [22], by which only several low-order correlations might be sufficient to describe a quantum state precisely under moderate nonlinearity. By tracking the evolution of these correlation functions, it is possible to solve the system dynamics efficiently in the classical-to-quantum crossover regime.

In this paper, the classical-to-quantum transition of nonlinear $\chi^{(2)}$ processes is investigated based on the quantum cluster-expansion (QCE) approach. In particular, we focus on degenerate $\chi^{(2)}$ interactions, including second-harmonic generation (SHG) and optical parametric oscillation (OPO) at different nonlinear coupling rates and pump powers. The numerical results show the deviation of the mean photon numbers and the quantum statistics from the predictions by

*lmwin@ustc.edu.cn
†clzou321@ustc.edu.cn

the classical theory, and manifest the classical-to-quantum transition when increasing the g/κ and the pump power. We developed the code for generating recursive QCE to arbitrary orders with an arbitrary number of modes. By comparing with the conventional numerical approaches based on master equations of truncated Hilbert space, the validity of QCE is verified and shows a factor 10^4 speedup under excitation of only 400 photons. Our approach is efficient for solving the problems with large intracavity photon numbers and also moderate g/κ ratio, and could be extended to study the quantum behaviors of other complex nonlinear optics systems.

II. PRINCIPLE OF QCE

In resonance-enhanced nonlinear photonics processes such as three-wave mixing and frequency comb generation in microrings [23], there are multiple optical resonances simultaneously satisfying the energy and phase-matching conditions. These modes are generally described by the bosonic annihilation operators O_j, where j labels individual mode, and any given system operator could be written as the product of a cluster of mode operators $A = \Pi_{j,k} O_j^{\dagger m_j} O_k^{n_k}$, which is a Mth-order operator with $M = \sum_j m_j + \sum_k n_k$. For an open quantum system, the dynamics of an operator A follows the master equation [3]

$$\frac{d}{dt}\rho = -\frac{i}{\hbar}[H, \rho] + \sum_j \kappa_j \mathcal{L}_{d_j}[\rho], \tag{1}$$

where ρ is the density matrix and H is the Hamiltonian of the system, κ_j is the dissipation rate, and $\mathcal{L}_{d_j}[\rho] = 2d_j\rho d_j^\dagger - d_j^\dagger d_j \rho - \rho d_j^\dagger d_j$ is the Lindblad operator for a jump operator d_j. For example, in the case of a reservoir with near-zero thermal excitation, the amplitude dissipation of individual modes is $\kappa_j \mathcal{L}_{d_j}[\rho]$. The expectation value of an operator $\langle A\rangle = \mathrm{Tr}\{A\rho\}$ also follows the master equation

$$\frac{d}{dt}\langle A\rangle = \frac{i}{\hbar}\langle [H, A]\rangle + \sum_j \kappa_j \langle \mathcal{L}'_{d_j}[A]\rangle, \tag{2}$$

where $\mathcal{L}'_{d_j}[A] = 2d_j^\dagger A d_j - d_j^\dagger d_j A - A d_j^\dagger d_j$.

The master equation shows that the dynamics of the expectation value of the Mth-order cluster A is directly coupled to operators $[H, A]$ and also $\mathcal{L}_{d_j}[A]$. For a simple bilinear Hamiltonian that consists of only second-order clusters, the evaluation of O_j only depends on the first-order clusters, thus the master equations of the system become an array of closed-form linear equations of O_j and $O_j^\dagger$, as shown by Fig. 1(a). The expectations of all second-order clusters then can be derived based on this set of linear equations, which further gives the covariance matrix of the system [3]. If all the environment modes and the system initial states are Gaussian states, the expectation values of the higher-order clusters can be expressed in terms of the first- and second-order clusters [Fig. 1(b)], and the system quantum state evolution can be completely described by the covariance matrix. However, for the system that involves $\chi^{(2)}$ and higher-order nonlinear interactions, i.e., the H consists of third- or higher-order clusters, the dynamics of second-order clusters should depend on the higher-order clusters [Fig. 1(c)], and the evolution of all clusters in general

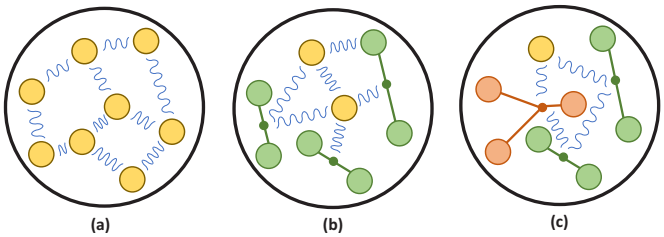

FIG. 1. Illustration of a quantum nonlinear system under different orders of quantum cluster expansion (QCE), with circles linked by straight lines denoting a cluster of bosonic operators and wavy lines coupling between clusters. (a) First-order QCE, corresponding to the mean-field approximation. (b) Second-order QCE. (c) Third-order QCE. For Mth-order QCE, the system is described by the dynamics of operators with orders no higher than M.

cannot be obtained in a closed form. For example, for the widely studied Kerr oscillator $H = g a^{\dagger 2} a^2$ with a coupling strength of g and mode dissipation rate κ_a, the evolution of the expectation value of a is governed by

$$\frac{d\langle a\rangle}{dt} = -2ig\langle a^\dagger a a\rangle - \kappa_a\langle a\rangle, \tag{3}$$

which requires us to track the value of a high-order operator $\langle a^\dagger a a\rangle$. Repeating the same process for $[H,\ a^\dagger a a]$ leads to an infinite hierarchy. Then the dynamics of $\langle a\rangle$ and $\langle a^\dagger a a\rangle$ are coupled with an infinite set of higher-order operators.

Two approaches can be applied to address this divergence of high-order operators.

(i) MFA, which neglects the fluctuations of strong fields and replaces them by complex numbers, thus reducing the order of clusters. In the classical limit, all operators are replaced by complex numbers, resulting in MFA shown in Fig. 1(a).

(ii) Fock-space truncation (FST). When the number of excitations in bosonic modes is restricted, the quantum state could be represented in the Fock basis with a finite dimension, and then the master equation could be solved numerically.

Although both approaches are widely adopted in quantum optics studies, they are not applicable to a system with moderate nonlinearities and strong drives.

Therefore, we revert to solve the original master equation with the QCE approach. In practice, it is unrealistic to track the expectation values of an infinite set of operators to evaluate the expectation value $\langle A\rangle$. Although the number of clusters involved for a complete system dynamics generally diverges, the QCE can be solved approximately or even analytically by truncating the order of QCE, i.e., setting the high-order clusters as zero. Such treatment has been established in quantum chemistry [24] and semiconductor systems [25,26] as well as Bose-Einstein condensates beyond the mean-field theory [27]. Different from these previous studies, the order of the hierarchy of a multimode nonlinear photonic system depends on the specific nonlinear processes involved. At large mode number and orders, the expansion of the clusters increases drastically, and it is intractable to directly write down all the equations for clusters and solve them analytically.

The high-order correlation is directly related to the nonlinear coupling rate g. In the weak-coupling limit $g \ll \kappa$,

the correlation between different operators can be neglected. The expectation values of Nth-order operators can be directly factorized to the product of first-order operators by

$$\langle\widehat{N}\rangle \approx \prod_{j=1}^{N}\langle O_j\rangle, \tag{4}$$

which is the main assumption of the MFA. At this limit, the photonic modes are treated as harmonic oscillators and the optical fields can be approximated to coherent states, as has been adopted by most experiments. The system dynamics is described by a set of nonlinearly coupled equations only containing the expectation values of first operators [Fig. 1(a)], while the tiny quantum fluctuation around the mean field $\langle O_j\rangle$ is neglected. As the g/κ ratio increases, the strong anharmonicity leads to the distortion of the quantum state from the coherent state, in which case the quantum correlation becomes significant so that the high-order correlation cannot be directly factorized to the product of single-order operators represented by Eq. (4). For example, a second-order operator can be written as $\langle\widehat{2}\rangle = \langle\widehat{1}\rangle\langle\widehat{1}\rangle + \Delta\langle\widehat{2}\rangle = \langle\widehat{2}\rangle_s + \Delta\langle\widehat{2}\rangle$, where $\langle\widehat{2}\rangle_s$ represents the MFA approximation by Eq. (4) and $\Delta\langle\widehat{2}\rangle$ indicates the purely correlated part. Likewise, the factorization of a Nth-order cluster reads

$$\begin{aligned}\langle\widehat{N}\rangle &= \langle\widehat{N}\rangle_s + \langle\widehat{N}-2\rangle_s\Delta\langle\widehat{2}\rangle + \langle\widehat{N}-4\rangle_s\Delta\langle\widehat{2}\rangle\Delta\langle\widehat{2}\rangle \\ &\quad + \ldots\Delta\langle\widehat{N}\rangle \\ &= \langle O_n\rangle\langle\widehat{N}-1\rangle + \Delta\langle O_n\widehat{1}\rangle\langle\widehat{N}-2\rangle \\ &\quad + \Delta\langle O_n\widehat{2}\rangle\langle\widehat{N}-3\rangle + \ldots\Delta\langle\widehat{N}\rangle,\end{aligned} \tag{5}$$

where each product term presents one factorization and is summed over all indistinguishable combinations. $\widehat{k}\,(0 < k \leqslant N)$ denotes all the possible ith-order clusters within the Nth-order cluster. And $\widehat{N}-k$ represents the remaining $(N-k)$th-order cluster. The second equality can be derived from Bell's number: All the indistinguishable expansions of the nth-order cluster can be mapped one to one onto the nth Bell number B_n, which has a recursion formula, $B_n = \sum_{k=0}^{n-1} C_{n-1}^{k} B_k$, $B_0 = 1$, where each term in the formula represents a unique factorization and decomposes the Nth-order cluster into two parts. For example, $C_{n-1}^{n-1-k}B_{n-1-k}$ represents the factorization into $\Delta\langle O_n\widehat{k}\rangle$ and $\langle\widehat{N}-1-k\rangle$, where $\widehat{k}$ denotes all the possible combinations of the ordered kth-order cluster. To give a concrete illustration of Eq.(5), we consider the expansion of a third-order cluster $\langle O_3O_2O_1\rangle$ as follows:

$$\begin{aligned}\langle O_3O_2O_1\rangle &= \langle O_3\rangle\langle O_2O_1\rangle + \Delta\langle O_3O_2\rangle\langle O_1\rangle \\ &\quad + \Delta\langle O_3O_1\rangle\langle O_2\rangle + \Delta\langle O_3O_2O_1\rangle \\ &= \langle O_3\rangle\langle O_2O_1\rangle + (\langle O_3O_2\rangle - \langle O_3\rangle\langle O_2\rangle)\langle O_1\rangle \\ &\quad + (\langle O_3O_1\rangle - \langle O_3\rangle\langle O_1\rangle)\langle O_2\rangle + \Delta\langle O_3O_2O_1\rangle \\ &= \langle O_3\rangle\langle O_2O_1\rangle + \langle O_1\rangle\langle O_3O_2\rangle + \langle O_2\rangle\langle O_3O_1\rangle \\ &\quad - 2\langle O_3\rangle\langle O_2\rangle\langle O_1\rangle + \Delta\langle O_3O_2O_1\rangle,\end{aligned} \tag{6}$$

where the pure correlation term $\Delta\langle O_3O_2O_1\rangle$ can be neglected for the second-order truncation.

Based on Eqs. (2) and (5), the dynamics of a nonlinear system can be implemented following the Mth-order QCE.

(1) To get the expectation value of $\langle\widehat{N}\rangle$, submit $\langle\widehat{N}\rangle$ to Eq. (2) and one gets its relation with $\langle\widehat{N}\rangle = \langle[H,N]\rangle$ and operator $\langle\widehat{i}\rangle$ of other orders.

(2) Following the Mth truncation that all $\Delta\langle\widehat{N}\rangle = 0$ for $N \geqslant M$, $\langle\widehat{N}\rangle$ and $\langle\widehat{i}\rangle$ can be factorized according to Eq. (5).

(3) Repeat steps 1 and 2 for any cluster that appears in step 2 until no new clusters are generated. In this way, we arrive at a set of nonlinear coupled equations involving clusters up to Mth order.

For the case of the Kerr oscillator in Eq. (3), the whole set of evolution equations under second-order truncation can be given following the above procedure as

$$\begin{aligned}\frac{d\langle a\rangle}{dt} &= -2ig(2\langle a^\dagger a\rangle\langle a\rangle + \langle a^2\rangle\langle a^\dagger\rangle - 2\langle a^\dagger\rangle\langle a\rangle^2) - \kappa_a\langle a\rangle, \\ \frac{d\langle a^2\rangle}{dt} &= -4ig(3\langle a^\dagger a\rangle\langle a^2\rangle - 2\langle a^\dagger\rangle\langle a\rangle^3) - 2(\kappa_a + ig)\langle a^2\rangle, \\ \frac{d\langle a^\dagger a\rangle}{dt} &= -2\kappa_a\langle a^\dagger a\rangle.\end{aligned} \tag{7}$$

In these equations, the expectation value of the Hermitian conjugate of an operator O fulfills $\langle O^\dagger\rangle = \langle O\rangle^*$. Generally, the number of equations will increase with the number of modes involved in the nonlinear interaction and the truncation order, making it inconvenient to give their explicit forms. Thus we implement an open-source package to automatically complete the factorization and calculation procedures. The technical details about the code and the data of our paper are available in Ref. [28].

III. CLASSICAL-TO-QUANTUM TRANSITION OF $\chi^{(2)}$ INTERACTION

We apply the QCE approach to investigate the classical-to-quantum transition of a signature quantum nonlinear optical system—degenerate $\chi^{(2)}$ interaction—involved in the SHG and OPO. For the phase-matched degenerate $\chi^{(2)}$ interaction between modes a and b, the interaction Hamiltonian in the rotating framework can be written as ($\hbar = 1$) [23,29]

$$H_I = \Delta_a a^\dagger a + \Delta_b b^\dagger b + g(a^{\dagger 2}b + a^2 b^\dagger), \tag{8}$$

where a (b) and $a^\dagger$ ($b^\dagger$) are the annihilation and creation operator of the fundamental (second-harmonic) mode with $\Delta_{a(b)}$ being the corresponding frequency detunings. g is the nonlinear coupling strength that depends on the material and cavity geometry. Under coherent drives, the corresponding excitation Hamiltonian reads

$$H_{\rm ex} = E_a(a^\dagger + a) + E_b(b^\dagger + b). \tag{9}$$

Here, $E_{a(b)}$ is the driving strength on mode $a(b)$. In the case of SHG, only mode a is pumped and thus we set $E_b = 0$, while E_a is set to be zero similarly for OPO. To simplify notation, we will simply use E to denote the corresponding pump amplitude in each case in the following text. In addition, each mode of the system experiences mode dissipation described by the Lindblad operator $\mathcal{L}_{a(b)}[.]$ with dissipation rate $\kappa_{a(b)}$.

For the MFA widely used in classical nonlinear optics, the dynamics of the system can be easily derived from Eq. (2) by

neglecting all the correlators as follows:

$$\begin{aligned}\frac{d\alpha}{dt} &= -(i\Delta_a+\kappa_a)\alpha - 2ig\beta\alpha^* - iE_a,\\ \frac{d\beta}{dt} &= -(i\Delta_b+\kappa_b)\beta - 2ig\alpha^2 - iE_b,\end{aligned} \tag{10}$$

where $\alpha(\beta)$ is the classical amplitude for mode $a(b)$. The classical model defined by the above equations infers that each mode can be fully described via a single c-number under the assumption that the system stays close to the two-mode separable coherent state, which we will prove to be invalid for strong nonlinear coupling strength.

Similarly to the case of the Kerr oscillator, QCE under second-order truncation gives rise to eight equations describing the system dynamics:

$$\begin{aligned}\frac{d\langle a\rangle}{dt} &= -(i\Delta_a+\kappa_a)\langle a\rangle - 2ig\langle ba^\dagger\rangle - iE_a,\\ \frac{d\langle b\rangle}{dt} &= -(i\Delta_b+\kappa_b)\langle b\rangle - ig\langle a^2\rangle - iE_b,\\ \frac{d\langle a^\dagger a\rangle}{dt} &= +iE_a(\langle a\rangle - \langle a^\dagger\rangle) - 2\kappa_a\langle a^\dagger a\rangle + 4g\mathrm{Im}[\langle a^{\dagger 2}\rangle\langle b\rangle + 2\langle a^\dagger b\rangle\langle a^\dagger\rangle - 2\langle a^\dagger\rangle^2\langle b\rangle],\\ \frac{d\langle b^\dagger b\rangle}{dt} &= +iE_b(\langle b\rangle - \langle b^\dagger\rangle) - 2\kappa_b\langle b^\dagger b\rangle - 2g\mathrm{Im}[\langle a^{\dagger 2}\rangle\langle b\rangle + 2\langle a^\dagger b\rangle\langle a^\dagger\rangle - 2\langle a^\dagger\rangle^2\langle b\rangle],\\ \frac{d\langle a^2\rangle}{dt} &= -2iE_a\langle a\rangle - 2(\kappa_a+i\Delta_a)\langle a^2\rangle - 2ig[(2\langle a^\dagger a\rangle+1)\langle b\rangle + 2\langle a^\dagger b\rangle\langle a\rangle + 2\langle a\, b\rangle\langle a^\dagger\rangle - 4\langle a^\dagger\rangle\langle a\rangle\langle b\rangle],\\ \frac{d\langle b^2\rangle}{dt} &= -2iE_b\langle b\rangle - 2(\kappa_b+i\Delta_b)\langle b^2\rangle - 2ig(\langle a^2\rangle\langle b\rangle + 2\langle a\, b\rangle\langle b\rangle - 2\langle a\rangle^2\langle b\rangle),\\ \frac{d\langle ab\rangle}{dt} &= -i(E_a\langle b\rangle + E_b\langle a\rangle) - (\kappa_a+\kappa_b+i\Delta_a+i\Delta_b)\langle ab\rangle - ig(3\langle a^2\rangle\langle a\rangle + 2\langle bb\rangle\langle a^\dagger\rangle + 4\langle a^\dagger b\rangle\langle b\rangle - 2\langle a\rangle^3 - 4\langle a^\dagger\rangle\langle b\rangle^2),\\ \frac{d\langle a^\dagger b\rangle}{dt} &= +i(E_a\langle b\rangle - E_b\langle a\rangle) + (i\Delta_a-\kappa_a-\kappa_b-i\Delta_b)\langle a^\dagger b\rangle,\\ &\quad - ig[2(\langle a^\dagger a\rangle - \langle b^\dagger b\rangle)\langle a\rangle + \langle a^2\rangle\langle a^\dagger\rangle - 2\langle ab^\dagger\rangle\langle b\rangle - 2\langle ab\rangle\langle b^\dagger\rangle + (4\langle b^\dagger\rangle\langle b\rangle - 2\langle a^\dagger\rangle\langle a\rangle)\langle a\rangle].\end{aligned} \tag{11}$$

Since the implementation of QCE with higher truncation orders is too complicated, we use a program to automatically perform the factorization and derivations [28].

Based on the QCE, we calculate the dynamics of the intracavity photon numbers $N_a = \langle a^\dagger a\rangle$ in mode a $N_b = \langle b^\dagger b\rangle$ in mode b for SHG, as summarized in Fig. 2 To demonstrate the validity the QCE, we compare the system evolution modeled by three different approaches. The master equation provides the most rigorous solution as long as the FST has the truncated dimension large enough. Under weak drive strength, we take the truncation dimension as 40 and 20 for mode a and mode b, respectively, and the computation is performed using QUTIP [34]. For comparison, the QCE is solved with the fourth-order truncation of clusters. The classical MFA model governed by Eqs.(10) is also evaluated, and we note that the MFA is actually the first-order QCE. For $E = 6$ and $g = 0.4$, with initial vacuum state, the dynamics of photon numbers in the two modes show excellent agreement between QCE and FST. However, the results of MFA deviate from the other two approaches, indicating that non-negligible quantum correlations between modes exist for $g/\kappa \sim 0.4$ as such effects could not be captured by the MFA. Additionally, the steady-state populations in two modes are studies for various g and E. Figures 2(c) and 2(d) show that the MFA and QCE start to deviate when g exceeds 0.1, indicating a crossover from classical to quantum regime. Similar behavior is shown when increasing E for a fixed $g = 0.2$, as shown in Figs. 2(e) and 2(f). Furthermore, MFA predicts a classical threshold above which it will lead to self-pulsing as marked in the shadow region. The critical driving strength E_c is given by

$$E_c = \frac{(2\kappa_a+\kappa_b)}{2g}\sqrt{2\kappa_b(\kappa_a+\kappa_b)}, \tag{12}$$

while it can be seen that the result above this threshold does not correspond with the ones offered by either QCE or FST.

For the OPO process, as shown in Fig. 3, the MFA predictions also significantly deviate from those of FST and QCE. When varying g and E, the deviation is only obvious at moderate values around the OPO threshold. As correctly predicted by MFA, degenerate OPO exhibits threshold driving strength E_c as

$$E_c = \frac{\kappa_a\kappa_b}{2g}, \tag{13}$$

similar to a second-order phase transition [30]. However, after taking the quantum correlation into consideration in the QCE, the intracavity photon number $\langle a^\dagger a\rangle$ and $\langle b^\dagger b\rangle$ changes smoothly with the driving strength E, in contrast to the sharp transition predicted by the MFA [Fig. 3(c)]. Due to the quantum fluctuation of the vacuum field, the spontaneous parametric down-conversion always generates photons in the fundamental mode a, which leads to the nonzero value of $\langle a^\dagger a\rangle$ for $E < E_c$. Even though semiclassical modification can be introduced to MFA to explain the spontaneous parametric oscillation, it is still difficult to predict the system behavior precisely when the drive amplitude is around the

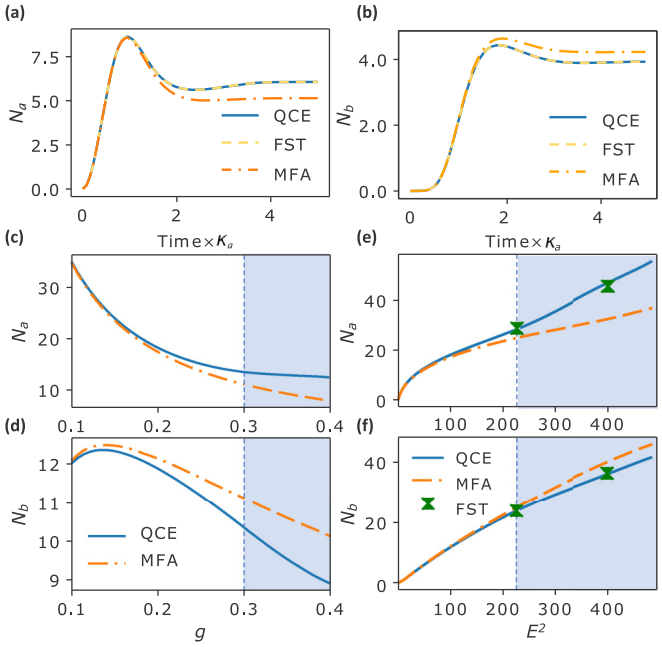

FIG. 2. Quantum-to-classical transition behaviors of second-harmonic generation. (a, b) The dynamical evolution of intracavity photon numbers $N_a = \langle a^\dagger a\rangle$ and $N_b = \langle b^\dagger b\rangle$ for two modes, with $E = 6$ and $g = 0.4$. (c, d) Steady-state intracavity photon number vs the coupling strength g, with $E = 10$. (e, f) Steady-state intracavity photon number vs the external drive strength E, with $g = 0.2$. In all calculations, $\kappa_a = \kappa_b = 1$ and the evolution duration of the system is $T_{\rm SS} = 10/\kappa_a$ which is long enough for the system to reach the steady state. Solid lines, dashed lines, and dash-dotted lines correspond to results obtained via fourth-order QCE, FST, and MFA, respectively. The shadow region denotes parameter spaces that lead to self-pulsing behavior predicted by MFA.

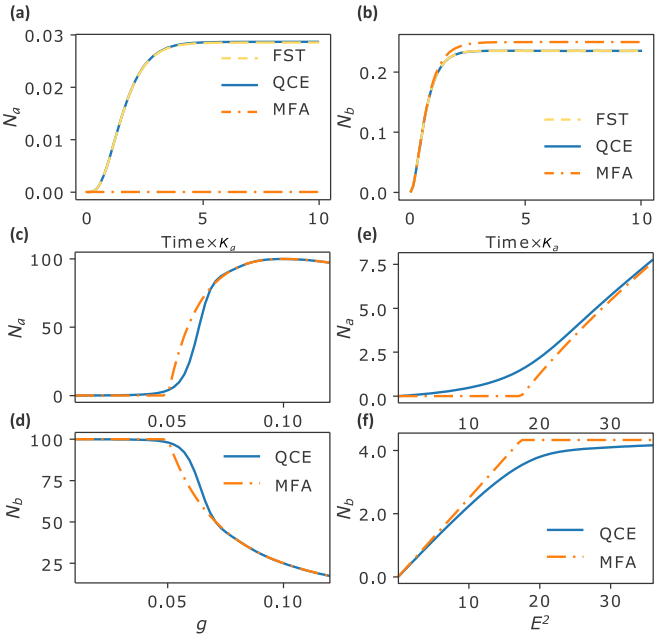

FIG. 3. Quantum-to-classical transition behaviors of optical parametric oscillation. (a, b) The dynamical evolution of cavity photon numbers $N_a = \langle a^\dagger a\rangle$ and $N_b = \langle b^\dagger b\rangle$ for two modes, with $E = 1$ and $g = 0.24$. (c, d) The steady-state cavity photon number against the coupling strength g, with $E = 20$. (e, f) The steady-state cavity photon number against the external drive strength E, with $g = 0.24$. In all calculations, $\kappa_a = \frac{1}{2}\kappa_b = 1$ and the evolution duration of the system is set to $T_{\rm SS} = 10/\kappa_a$. Solid lines, dashed lines, and dash-dotted lines correspond to the results via fourth-order QCE, FST, and MFA, respectively.

threshold. For both SHG and OPO, MFA is consistent with other approaches at the weak-coupling limit, thus validating the coupled-mode theory widely adopted for nonlinear optical systems with $g/\kappa \ll 1$. For OPO far above threshold (E and g are large enough), the photon number in the fundamental mode is much larger than the second-harmonic mode, thus their quantum correlation can be safely neglected, i.e., $\Delta\langle\hat{2}\rangle \approx 0$. In this case, QCE and MFA agree with each other.

Besides offering more accurate prediction of the photon numbers, another prominent advantage of the QCE is its ability to track the quantum statistics of the optical fields when the nonlinear optical system transits from weakly anharmonic to strongly anharmonic regime. In quantum optics, the equal-time second-order self-correlation function

$$g^{(2)}(0) = \frac{\langle O^\dagger O^\dagger O O\rangle}{\langle O^\dagger O\rangle^2} \tag{14}$$

is often used to quantify the quantum statistics of a mode O. It requires the operator cluster to be truncated at least to the second order, whereas MFA could not track the correlation functions since $\langle O^\dagger O^\dagger O O\rangle = \langle O^\dagger O\rangle^2$ for first-order truncation. In contrast to the coupled-mode equations by MFA, which can be transformed to g/κ-invariant form [31], the quantum correlation function is coupled with the mean fields in QCE, and thus depends on the pump power and g/κ. It is worth noting that the QCE also enables the calculation of arbitrary high-order quantum correlation functions by choosing an appropriate truncation order.

Figure 4 shows $g^{(2)}(0)$ as a function of the coupling strength g and the driving strength E. For SHG, the $g^{(2)}(0)$

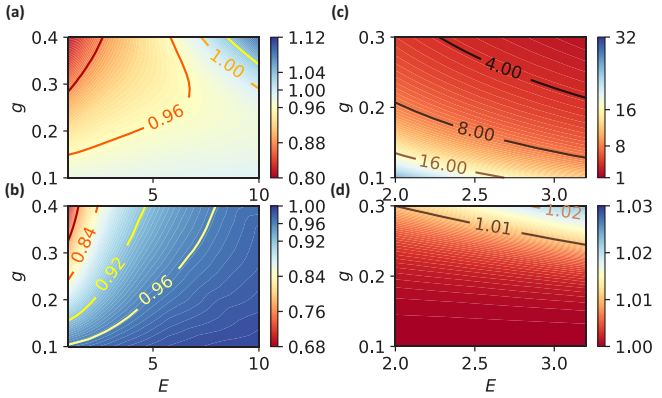

FIG. 4. Quantum second-order correlation function $[g^{(2)}(0)]$ of different modes calculated by sixth-order quantum-cluster expansion with varying coupling rate g and driving strength E. (a, b) The $g^{(2)}(0)$ for modes a and b, respectively, under the SHG drive $\kappa_a = \kappa_b = 1$. (c, d) The $g^{(2)}(0)$ for modes a and b, respectively, under the OPO drive $\kappa_a = \frac{1}{2}\kappa_b = 1$. For all calculation, the evolution duration of the system is set to $T_{\rm SS} = 10/\kappa_a$.

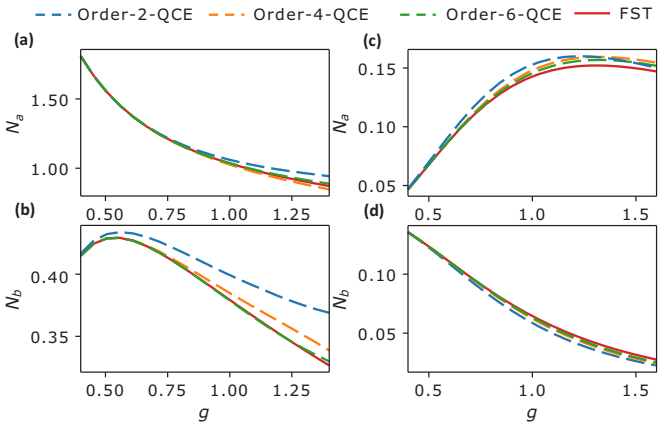

FIG. 5. The performance of the QCE approach of different orders. (a, b) Steady-state intracavity photon number of modes a and b, under the SHG drive $E = 2$ with $\kappa_a = \kappa_b = 1$. (c, d) Steady-state photon number of modes a and b, under the OPO drive intensity $E = 0.8$ with $\kappa_a = \frac{1}{2}\kappa_b = 1$. The solid lines are the reference results calculated by FST.

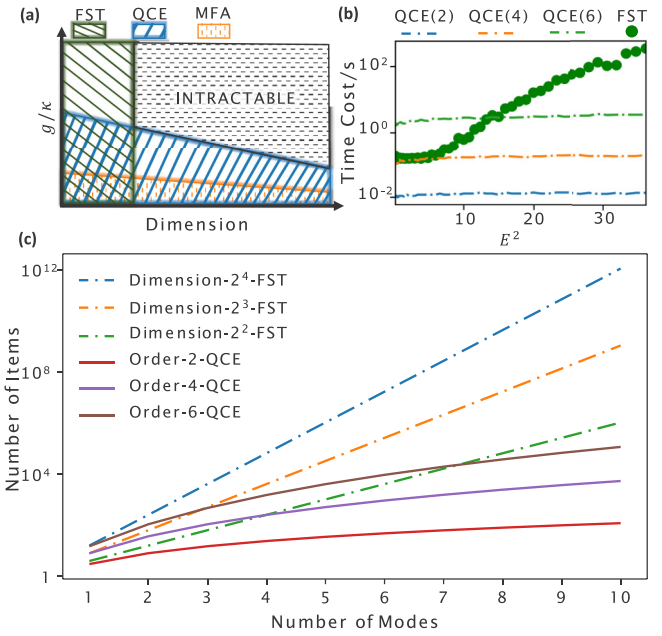

FIG. 6. Time consumption and computational complexity for different approaches. (a) Qualitative illustration of the applicable parameter regions of FST, QCE, and MFA. (b) The computation time of the SHG model via FST compared with that via QCE with different orders on a personal computer. The truncation dimension of FST is $\max(E^2, 4) \times \frac{1}{2}\max(E^2, 4)$. (c) The computational complexity of multimode systems. Solid lines and dash-dotted lines are the numbers of items of the partial differential equations for QCE with different truncation orders and the FST with different truncation dimensions.

functions of the fundamental and SH mode are smaller than 1 when g is large and E is small, revealing the photon antibunching due to the significant quantum photon blockade effect [20,21]. As the driving strength E becomes large, the $g^{(2)}(0)$ function tends above 1, which corresponds to the bunching effect and can be attributed to optical bistability and bifurcation [32,33]. The OPO case [Figs. 4(c) and 4(d)] also shows the pump power-dependent $g^{(2)}(0)$ function, which indicates the classical-to-quantum transition of OPO under a strong pump as the value of the $g^{(2)}(0)$ function diverges from 1.

IV. PERFORMANCE ANALYSIS

It is of great importance to gain further insights into the performance of QCE as the nonlinear optical system transitions from weakly harmonic ($g/\kappa \ll 1$) to strongly anharmonic ($g/\kappa \gg 1$) regime. Figure 5 shows the performances of QCE for SHG and OPO with different QCE truncation orders. The solid line is obtained by solving the master equation in the Fock-state basis and is used as a reference. For both SHG and OPO, the deviations of the QCE results become large with the increase of the coupling strength g, indicating an increased high-order quantum correlation. It is anticipated that it is more accurate to treat the nonlinear system as multilevel atoms when $g/\kappa \gg 1$ [19]. By expanding the operator clusters to higher order, the results of QCE, as shown by the dashed curves with orders of 2, 4, and 6, converge to the result of the FST. However, as the order of expansion increases, a much larger number of clusters are involved in the nonlinear coupled equation, and lead to exceptionally high computational complexity, especially for $g \gg \kappa$.

Therefore, the potential advantage of the QCE approach is discussed by comparing its time consumption and computational complexity with other approaches. In a nutshell, Fig. 6(a) offers a qualitative illustration of the applicable parameter region for the three methods discussed in this paper. The MFA is efficient and accurate for very weak nonlinearity with $g/\kappa \ll 1$. For the FST, the density matrix contains the full information of the optical fields with a finite Fock-space dimension, and can be used for the calculation of the expectation value of operators with arbitrarily high order. Thus, the FST method is particularly powerful for $g/\kappa \gg 1$, since only a small amount of photon number states is enough to capture the system's behavior due to the strong anharmonicity, but is limited to very few modes. The QCE is more suitable for nonlinear systems with moderate nonlinearity $g/\kappa \lesssim 1$, and its superiority is particularly significant for strong pump power and large mode number. For example, in Fig. 2 with $g/\kappa = 0.2$, a fourth-order QCE is enough to predict the photon numbers of both modes with high precision. The star marked near the curve of QCE [Fig. 2(d)] presents the result of FST in a dimension of 100×100, which costs nearly 12 h for Monte Carlo simulations [31] of 2000 trajectories by Qutip [34]. In contrast, there are only 37 clusters in the fourth-order QCE used, and the calculation takes only 1 s on the same computer, showing a factor 10^4 speedup.

Figure 6(b) shows the quantitative result for the time cost to complete a single simulation task via FST and QCE of different orders. It is clear that the time cost for FST increases exponentially with the pump power while the time costs for QCE approaches are almost constants. Furthermore, the two approaches scale differently with the system dimension, as shown in Fig. 6(c). For the open system with m modes, the number of equations to solve with FST is n_{trunc}^m,

which increases exponentially with m (dashed lines). Thus, the FST approach becomes impractical when the photon number exceeds 1000 for $m \geqslant 5$, as implied by the quantum supremacy [35]. Fortunately, for the QCE, the exponential scaling is reduced down to the polynomial relationship between the number of clusters and the number of modes, as shown by the solid lines in Fig. 6(c). To the second-order expansion, the maximum number of items $f^{(2)}(m)$ tracked in the differential equations is $m^2 + 2m$, which grows quadratically with mode number. For nth-order expansion, the number of items is still a polynomial function of mode number with $O(m^n)$. Even though these clusters couple with each other nonlinearly, the computation complexity still follows a polynomial relationship with the number of modes, thus demonstrating the superiority of QCE for quantum many-body physics in multimode bosonic systems.

V. CONCLUSION

In summary, we use the quantum cluster-expansion approach to investigate the classical-to-quantum transition of multimode nonlinear optical systems. The $\chi^{(2)}$ nonlinearity is investigated as a signature two-mode system, with pump laser driving either the fundamental mode or second-harmonic mode. We have discussed the system dynamics with various nonlinear coupling strengths to dissipation ratio g/κ, and different approaches including the MFA, FST, and QCE are numerically implemented and compared. It is found that the QCE approach could bridge the gap between the MFA and FST, i.e., capture both the classical behaviors and the quantum correlations between modes, and is appropriate for the nonlinear optical system with a large number of modes and also relatively strong excitations with $g/\kappa \lesssim 1$. QCE greatly reduces the computational complexity and can be applied to describe a wide range of applications based on bosonic oscillators with moderate anharmonicity, including the rapidly developing integrated nonlinear photonics [15–17,36] and the superconducting cavity with kinetic inductance [37,38]. The experimental progress raises an urgent need for the theoretical simulation of nonlinear photonic systems with high efficiency.

ACKNOWLEDGMENTS

Y.-X.H. thanks Qianhui Lu and Mingda Li for their support and inspiring ideas in numerical calculations. This work was funded by the National Key R&D Program (Grant No. 2017YFA0304504), the National Natural Science Foundation of China (Grants No. 11874342, No. 11922411, No. 12061131011, No. 11904316, and No. U21A20433), and the Natural Science Foundation of Anhui Province (Grants No. 2008085QA34 and No. 2108085MA17). M.L. and C.L.Z. were also supported by the Fundamental Research Funds for the Central Universities, and the State Key Laboratory of Advanced Optical Communication Systems and Networks. The numerical calculations in this paper were partially done on the supercomputing system in the Supercomputing Center of University of Science and Technology of China.

[1] R. W. Boyd, *Nonlinear Optics* (Academic, New York, 2003).
[2] G. P. Agrawal, *Nonlinear Fiber Optics* (Springer, New York, 2000).
[3] D. F. Walls and G. J. Milburn, *Quantum Optics* (Springer, New York, 2007).
[4] X.-B. Wang, T. Hiroshima, A. Tomita, and M. Hayashi, Quantum information with gaussian states, Phys. Rep. **448**, 1 (2007).
[5] C. Weedbrook, S. Pirandola, R. Garcia Patron, N. J. Cerf, T. C. Ralph, J. H. Shapiro, and S. Lloyd, Gaussian quantum information, Rev. Mod. Phys. **84**, 621 (2012).
[6] D. F. Walls, Squeezed states of light, Nature (London) **306**, 141 (1983).
[7] S. L. Braunstein and P. Van Loock, Quantum information with continuous variables, Rev. Mod. Phys. **77**, 513 (2005).
[8] D. Vitali, S. Gigan, A. Ferreira, H. R. Böhm, P. Tombesi, A. Guerreiro, V. Vedral, A. Zeilinger, and M. Aspelmeyer, Optomechanical Entanglement between a Movable Mirror and a Cavity Field, Phys. Rev. Lett. **98**, 030405 (2007).
[9] C.-L. Zou, X.-B. Zou, F.-W. Sun, Z.-F. Han, and G.-C. Guo, Room-temperature steady-state optomechanical entanglement on a chip, Phys. Rev. A **84**, 032317 (2011).
[10] S. Krastanov, M. Heuck, J. H. Shapiro, P. Narang, D. R. Englund, and K. Jacobs, Room-temperature photonic logical qubits via second-order nonlinearities, Nat. Commun. **12**, 191 (2021).
[11] L. Chang, A. Boes, P. Pintus, J. D. Peters, M. Kennedy, X.-W. Guo, N. Volet, S.-P. Yu, S. B. Papp, and J. E. Bowers, Strong frequency conversion in heterogeneously integrated gaas resonators, APL Photonics **4**, 036103 (2019).
[12] A. W. Bruch, X. Liu, X. Guo, J. B. Surya, Z. Gong, L. Zhang, J. Wang, J. Yan, and H. X. Tang, 17000%/w second-harmonic conversion efficiency in single-crystalline aluminum nitride microresonators, Appl. Phys. Lett. **113**, 131102 (2018).
[13] M. Zhao and K. Fang, Nanophotonic integrated circuits with 1% single-photon nonlinearity, arXiv:2105.12705.
[14] J. Lu, J. B. Surya, X. Liu, A. W. Bruch, Z. Gong, Y. Xu, and H. X. Tang, Periodically poled thin-film lithium niobate microring resonators with a second-harmonic generation efficiency of 250, 000%/w, Optica **6**, 1455 (2019).
[15] J. Lin, N. Yao, Z. Hao, J. Zhang, W. Mao, M. Wang, W. Chu, R. Wu, Z. Fang, L. Qiao, W. Fang, F. Bo, and Y. Cheng, Broadband Quasi-Phase-Matched Harmonic Generation in an On-Chip Monocrystalline Lithium Niobate Microdisk Resonator, Phys. Rev. Lett. **122**, 173903 (2019).
[16] J.-Y. Chen, Z. Li, Z. Ma, C. Tang, H. Fan, Y. M. Sua, and Y.-P. Huang, Photon Conversion and Interaction in a Quasi-Phase-Matched Microresonator, Phys. Rev. Appl. **16**, 064004 (2021).
[17] J. Lu, M. Li, C.-L. Zou, A. Al Sayem, and H. X. Tang, Toward 1% single-photon anharmonicity with periodically poled lithium niobate microring resonators, Optica **7**, 1654 (2020).
[18] W. T. M. Irvine, K. Hennessy, and D. Bouwmeester, Strong Coupling between Single Photons in Semiconductor Microcavities, Phys. Rev. Lett. **96**, 057405 (2006).

[19] M. Li, Y.-L. Zhang, H. X. Tang, C.-H. Dong, G.-C. Guo, and C.-L. Zou, Photon-Photon Quantum Phase Gate in a Photonic Molecule with $\chi^{(2)}$ Nonlinearity, Phys. Rev. Appl. **13**, 044013 (2020).

[20] S. Ferretti and D. Gerace, Single-photon nonlinear optics with kerr-type nanostructured materials, Phys. Rev. B **85**, 033303 (2012).

[21] A. Majumdar and D. Gerace, Single-photon blockade in doubly resonant nanocavities with second-order nonlinearity, Phys. Rev. B **87**, 235319 (2013).

[22] M. Kira and S. W. Koch, Cluster-expansion representation in quantum optics, Phys. Rev. A **78**, 022102 (2008).

[23] M. Li, C.-L. Zou, C.-H. Dong, X.-F. Ren, and D.-X. Dai, Enhancement of second-harmonic generation based on the cascaded second-and third-order nonlinear processes in a multimode optical microcavity, Phys. Rev. A **98**, 013854 (2018).

[24] F. E. Harris, H. J. Monkhorst, and D. L. Freeman, *Algebraic and Diagrammatic Methods in Many-Fermion Theory* (Dover, New York, 2020).

[25] M. Kira, W. Hoyer, T. Stroucken, and S. Koch, Exciton Formation in Semiconductors and the Influence of a Photonic Environment, Phys. Rev. Lett. **87**, 176401 (2001).

[26] M. Kira, F. Jahnke, and S. W. Koch, Quantum Theory of Secondary Emission in Optically Excited Semiconductor Quantum Wells, Phys. Rev. Lett. **82**, 3544 (1999).

[27] A. Vardi and J. Anglin, Bose-Einstein Condensates beyond Mean Field Theory: Quantum Backreaction as Decoherence, Phys. Rev. Lett. **86**, 568 (2001).

[28] Y.-X. Huang and K. Lin, QCLS, https://github.com/yesunhuang/QCLS.

[29] X. Guo, C. Zou, and H. Tang, Second-harmonic generation in aluminum nitride microrings with 2500%/ W conversion efficiency, Optica **3**, 1126 (2016).

[30] P. Drummond, K. McNeil, and D. Walls, Non-equilibrium transitions in sub/second harmonic generation, Opt. Acta **27**, 321 (1980).

[31] X. Zheng and C. Savage, Quantum trajectories and classical attractors in second-harmonic generation, Phys. Rev. A **51**, 792 (1995).

[32] C. M. Savage, Oscillations and quantized second-harmonic generation, Phys. Rev. A **37**, 158 (1988).

[33] S. Gevorkyan, Bifurcation and quantum delocalized states in second-harmonic generation, Phys. Rev. A **62**, 013813 (2000).

[34] J. R. Johansson, P. D. Nation, and F. Nori, Qutip 2: A python framework for the dynamics of open quantum systems, Comput. Phys. Commun. **184**, 1234 (2013).

[35] J. Preskill, Quantum computing and the entanglement frontier, arXiv:1203.5813.

[36] Z. Hao, L. Zhang, W. Mao, A. Gao, X. Gao, F. Gao, F. Bo, G. Zhang, and J. Xu, Second-harmonic generation using d33 in periodically poled lithium niobate microdisk resonators, Photon. Res. **8**, 311 (2020).

[37] Z. Wang, M. Pechal, E. A. Wollack, P. Arrangoiz-Arriola, M. Gao, N. R. Lee, and A. H. Safavi-Naeini, Quantum Dynamics of a Few-Photon Parametric Oscillator, Phys. Rev. X **9**, 021049 (2019).

[38] C. K. Andersen, A. Kamal, N. A. Masluk, I. M. Pop, A. Blais, and M. H. Devoret, Quantum Versus Classical Switching Dynamics of Driven Dissipative Kerr Resonators, Phys. Rev. Appl. **13**, 044017 (2020).